

Article

Improved A* Algorithm for Path Planning Based on CubeSats In-Orbit Electromagnetic Transfer System

Duo Xu, Honghao Yue, Yong Zhao , Fei Yang, Jun Wu, Xueting Pan, Tao Tang and Yuhao Zhang

School of Mechatronics Engineering, Harbin Institute of Technology, Harbin 150080, China

* Correspondence: 19b908114@stu.hit.edu.cn; Tel.: +86-133-2940-8782

Abstract: For future large-scale CubeSat applications in orbit, the deployer must accommodate a greater number of CubeSats and facilitate cluster releases. This paper introduces an improved A* algorithm tailored for CubeSat in-orbit transfer path planning. Unlike the traditional A* algorithm, this enhanced version incorporates a path coordination strategy to manage congestion caused by the simultaneous transfer of many CubeSats, ensuring they reach their designated release positions smoothly and thus significantly boosting the efficiency of CubeSat transfers. Additionally, the algorithm develops a cost model for attitude disturbances on the electromagnetic conveying platform and crafts an improved cost function. It strategically balances the reduction in attitude disturbances caused by CubeSat transfers with the efficiency of these transfers. The primary goal is to minimize platform disturbances while optimizing the number of steps CubeSats need to reach their intended positions. The effectiveness of this algorithm is demonstrated through detailed case studies, which confirm that during the CubeSat transfer process, the platform's attitude remains stable, and the transfer efficiency is well-managed, achieving efficient path planning for the in-orbit transfer of numerous CubeSats.

Keywords: improved A* algorithm; CubeSat in-orbit transfer; path planning; attitude disturbance



Citation: Xu, D.; Yue, H.; Zhao, Y.; Yang, F.; Wu, J.; Pan, X.; Tang, T.; Zhang, Y. Improved A* Algorithm for Path Planning Based on CubeSats In-Orbit Electromagnetic Transfer System. *Aerospace* **2024**, *11*, 394. <https://doi.org/10.3390/aerospace11050394>

Academic Editor: George Z. H. Zhu

Received: 16 April 2024

Revised: 8 May 2024

Accepted: 9 May 2024

Published: 15 May 2024



Copyright: © 2024 by the authors. Licensee MDPI, Basel, Switzerland. This article is an open access article distributed under the terms and conditions of the Creative Commons Attribution (CC BY) license (<https://creativecommons.org/licenses/by/4.0/>).

1. Introduction

CubeSats possess several advantages, including their compact size, being lightweight, and rapid development cycles. When deployed in groups, they can undertake complex tasks, such as constellation formation and formation flying, which would be challenging for a single large satellite [1,2]. Typically launched as secondary payloads using box-type deployers and released into orbit via internal springs, individual CubeSats reach their designated orbits. However, to accommodate the increasing demand for large-scale CubeSat applications, future deployers must support the deployment of a greater number of CubeSats and enable cluster releases in orbit [3].

The current multi-satellite deployment scheme primarily utilizes box-type deployers with compressed spring ejection mechanisms. Among the notable developments in this area, the P-POD CubeSat deployer stands out. Developed jointly by the California Institute of Technology and Stanford University in the United States, the P-POD is capable of accommodating three standard 1U CubeSats. It is the earliest developed and most widely used CubeSat release mechanism to date. To date, this deployer has successfully launched over 150 CubeSats into orbit [4–8]. The University of Toronto in Canada has developed the Generic Nanosatellite Bus (GNB), a deployment device specifically designed for releasing the CanX series nanosatellites, which are each sized at 200 mm × 200 mm × 200 mm [9,10]. The GNB deployer operates on a similar principle to the U.S. P-POD, but it features an open-sided casing that allows for the storage and deployment of nanosatellites equipped with antennas, enhancing its functionality. The DRAGON small satellite deployment device, pioneered by the Space Research Center of the Polish Academy of Sciences, is designed to release nanosatellites measuring 200 mm × 200 mm × 200 mm [11]. The

NASA WWF deployer accommodates rectangular payloads of $10 \times 23 \times 35$ cm and can release 6U CubeSats. Using linear springs for propulsion, this system halts the satellite midway to allow orbit-guidance systems to complete the trajectory [12]. Meanwhile, the JEM Small Satellite Orbital Deployer (J-SSOD), developed by the Japan Aerospace Exploration Agency, managed to separate 1U CubeSats weighing 1 kg from the International Space Station in 2015, achieving separation velocities between 1.1 m/s and 1.7 m/s. This deployer uses a box storage mechanism with compressed springs and linear guide rails to release up to three 1U CubeSats simultaneously [13]. Although the design of CubeSat box-type deployers is simple and well-researched, they have limitations, such as a maximum capacity of three 1U CubeSats and a lack of reusability. To deploy a large number of CubeSats simultaneously, the use of multiple deployers is required, which significantly increases space occupancy. Currently, to expand deployer capacity, configurations often involve either multi-row combinations or enlargements within a two-dimensional plane. Essentially, these setups integrate multiple single-row deployers, equipping each CubeSat with an independent launch window and separation mechanism. However, the constraints imposed by the separation mechanism's layout and operation hinder the possibility of three-dimensional deployer combinations or the direct, large-scale storage and release of stacked CubeSats. References [14–17] introduce a new deployment approach for large-scale, stacked CubeSats for in-orbit transfer and release. This scheme enhances storage capacity by tightly stacking CubeSats in three dimensions and utilizes the CubeSats in-orbit electromagnetic transfer system to methodically push these stacked CubeSats from a three-dimensional arrangement onto a two-dimensional transfer platform. The CubeSats are then moved to the release window using a planar two-dimensional drive, effectively transforming a three-dimensional transfer challenge into a two-dimensional platform issue. Due to the high number and significant mass of the CubeSats, dynamic shifts in the system's center of mass occur during the transfer process within the deployer. Additionally, the actuation forces generated during the movement can disturb the electromagnetic conveying platform's attitude and decrease pointing accuracy, resulting in discrepancies between the CubeSats' actual and intended positions post-separation. To tackle this, in-orbit path planning for CubeSats is essential to ensure the stability of the electromagnetic conveying platform's attitude during transfers. This strategic planning helps mitigate the effects of mass center shifts and actuation forces, thereby enhancing both the stability of the platform's attitude and the precision of CubeSat deployment.

For CubeSat in-orbit transfer path planning, the objective is to minimize disturbances to the electromagnetic conveying platform's attitude while also reducing the number of steps CubeSats need to reach their designated positions. This involves considering multiple factors such as transfer torque, the platform's angular velocity, and the number of CubeSat movement steps, making it a multi-objective path planning challenge. Researchers have developed several solutions to address this complex problem, including well-known algorithms like A*, ant colony optimization, and Dijkstra's algorithm. The A* algorithm is particularly noted for its efficiency in path optimization, as it integrates global information while assessing each potential node along the shortest path. It creates a cost function between the start and end points, estimates the distance from the current node to the endpoint, and uses this estimate to assess the node's likelihood of being on the shortest route. This targeted approach not only speeds up the search process but also makes it more directed [18]. Significant advancements have been made in refining the A* algorithm. For instance, Baoying Li et al. [19] enhanced the algorithm to address issues like redundant nodes, slow search speeds, and frequent abrupt turns, resulting in smoother paths for mobile robots. Huanwei Wang et al. [20] introduced modifications like extended distance, bidirectional search, and path smoothing methods to improve the algorithm's efficiency and decrease the number of sharp turns. Chenguang Liu et al. [21] tailored an improved A* algorithm for ship route planning to balance path length with navigation safety. Guozheng Fan et al. [22] tackled UAV path planning challenges such as computational burdens, response delays, and obstacle avoidance during missions with an improved

A* algorithm. Yunfeng Fan et al. [23] proposed an improved A* algorithm for multi-robot systems in warehouse logistics to ensure collision-free and optimal path planning for each robot. Similarly, Minghao Li et al. [24] developed a version of the A* algorithm to swiftly detect explosives in scenarios where their locations are unknown, demonstrating that this enhanced algorithm can find the shortest path faster and more efficiently than other models. Due to the traditional A* algorithm's issues with excessive path turning points and slow search speeds in spatial obstacle path planning, Yangqi Ou et al. [25] proposed an enhanced version of the A* algorithm, which incorporates a path smoothing strategy and an adaptive cost function into the traditional A* algorithm framework. These additions help reduce the number of path steps turning points and increase the search efficiency. Despite their effectiveness, these methods did not consider dynamic factors, which are crucial in the CubeSat in-orbit electromagnetic transfer system where path planning is based on dynamic models. Unlike other applications that prioritize shorter paths and quicker computation times, CubeSat path planning focuses on minimizing the impact on the electromagnetic conveying platform. The primary goal is to reduce disturbances during transfers, with the secondary aim of achieving shorter paths and faster execution times. Thus, dynamic parameters like transfer torque, angular velocity, and center of mass position are critical in selecting the most suitable CubeSat transfer paths, ensuring the stability and precision of the platform's operations.

Given the limitations of existing path planning algorithms, this paper proposes an improved A* algorithm to address the path planning problem for CubeSat in-orbit transfer. The improved A* algorithm considers both the degree of disturbance to the attitude of the electromagnetic conveying platform caused by CubeSat transfer and the efficiency of CubeSat transfer. It aims to minimize the disturbance to the attitude of the electromagnetic conveying platform while minimizing the number of steps required for CubeSats to reach their expected positions. The main contributions and innovations of the paper are the following three aspects:

(1) Establish a Cost Model for Attitude Disturbance: Develop a model considering dynamic parameters such as transfer torque, angular velocity, and angular acceleration that the electromagnetic conveying platform experiences. Determine the position of the center of mass to assess the extent of attitude disturbance caused by CubeSat transfers and refine the cost function based on these findings.

(2) Introduce Path Coordination Strategy: Adapt the traditional A* algorithm by incorporating a path coordination strategy. This strategy addresses potential blockages caused by other CubeSats during transfer, ensuring smooth progress to intended release positions and avoidance of local optima.

(3) Optimize Management of the Open List: Enhance the computational speed and search efficiency by pre-filtering node information in the open list to reduce its size.

The remainder of the paper is structured to provide a comprehensive overview of the CubeSat in-orbit transfer system, starting with Section 2, which introduces the working principles of the system and the initial environment modeling. Section 3 delves into the foundational principles and limitations of the traditional A* algorithm. In Section 4, enhancements made to the A* algorithm are detailed. Section 5 presents a comparative analysis of test results from the improved A* algorithm to determine the optimal transfer path for specific CubeSat scenarios. Finally, Section 6 concludes the paper with summarizing remarks.

2. The CubeSats In-Orbit Electromagnetic Transfer System and the Modeling of the Initial Environment

2.1. The Working Principle and the Mechanical Structure of the Transfer System

Currently, orbital deployers for CubeSats employ a deployment mechanism that combines compression spring ejection with rail guidance to facilitate the separation and release of CubeSats in space. However, the one-time operational capability of compression springs limits their use for the ongoing orbital transfer and release demands of CubeSats. Addition-

ally, compression springs only provide instantaneous force, which lacks the consistency required for controlled transfer and release operations tailored to CubeSats with varying mass specifications. After separation, CubeSats may exhibit significant angular and lateral velocities, posing challenges for the rapid execution of formation flying, accompanying maneuvers, and other coordinated space missions. Due to the mechanical characteristics of springs, compression springs are restricted to one-dimensional actuation, making them unsuitable for the two-dimensional transfer needs of CubeSats. This limitation confines them to release CubeSats in a single, unidirectional row, and they cannot perform counter-releases that would minimize torque and reduce disturbances to the electromagnetic conveying platform's attitude. In contrast, electromagnetic actuation offers two-dimensional transfer capabilities on the platform, provides a consistent force for separation, and supports the precise deployment of large quantities of CubeSats. This paper describes a large-scale CubeSats in-orbit transfer and release system that stacks CubeSats in high-density, three-dimensional configurations. Once in orbit, electromagnetic drive units inside the deployer facilitate multidimensional, parallel translational movement to the release window. Voice coil electromagnetic actuators then perform the separation and release of the CubeSats, efficiently deploying large clusters of payloads in orbit.

The CubeSats in-orbit transfer system is primarily composed of electromagnetic drive units, CubeSat trays, and integrated push plates, as illustrated in Figure 1a. First, the system deploys a large number of 1U, 2U, and 3U CubeSats in three columns, with the two-dimensional transfer platform at the bottom. The initial state is empty, as shown in Figure 1b. Upon receiving the CubeSat release command, the system uses the built-in pusher to push the CubeSats from top to bottom onto the transfer platform below, as shown in Figure 1c. Next, the in-orbit transfer paths for the CubeSats are developed by considering their relative positions to the release window. This planning process evaluates both the impact of the transfer on the electromagnetic conveying platform's attitude and the overall efficiency of the CubeSat transfer. Using electromagnetic drive units, the CubeSats are maneuvered with two degrees of freedom on a plane, guided along transfer tracks to reach the release window, as depicted in Figure 1d. The quantity and positioning of the release devices on the transfer platform significantly affect the platform's attitude, the efficiency of the CubeSat transfer, and the collision risks during the large-scale, simultaneous release. To minimize disturbances to the platform's attitude during the CubeSats' release, the system counterbalances the actuation forces from the release mechanisms by aligning the combined force of the release actuation with the platform's center of mass. This alignment ensures that the torque generated by these forces is minimized throughout the release process. Research and analysis of the actual situation of the electromagnetic conveying platform suggest that releasing four target CubeSats simultaneously poses a high collision risk. However, releasing them individually or in a staggered manner (relative to the velocity direction of 0° and 180°) lowers this risk [26–28]. For an 8×8 electromagnetic conveying platform, this paper proposes installing four release devices, releasing one pair of CubeSats first, followed by another pair after a safe interval, thus effectively minimizing collision risks associated with simultaneous releases. Finally, this paper discusses using a coil-type electromagnetic actuator that adjusts the separation force by controlling the current magnitude. This allows for speed-adjusted releases tailored to target CubeSats of different mass specifications, facilitating the on-orbit cluster deployment of large batches of payloads, as shown in Figure 1e.

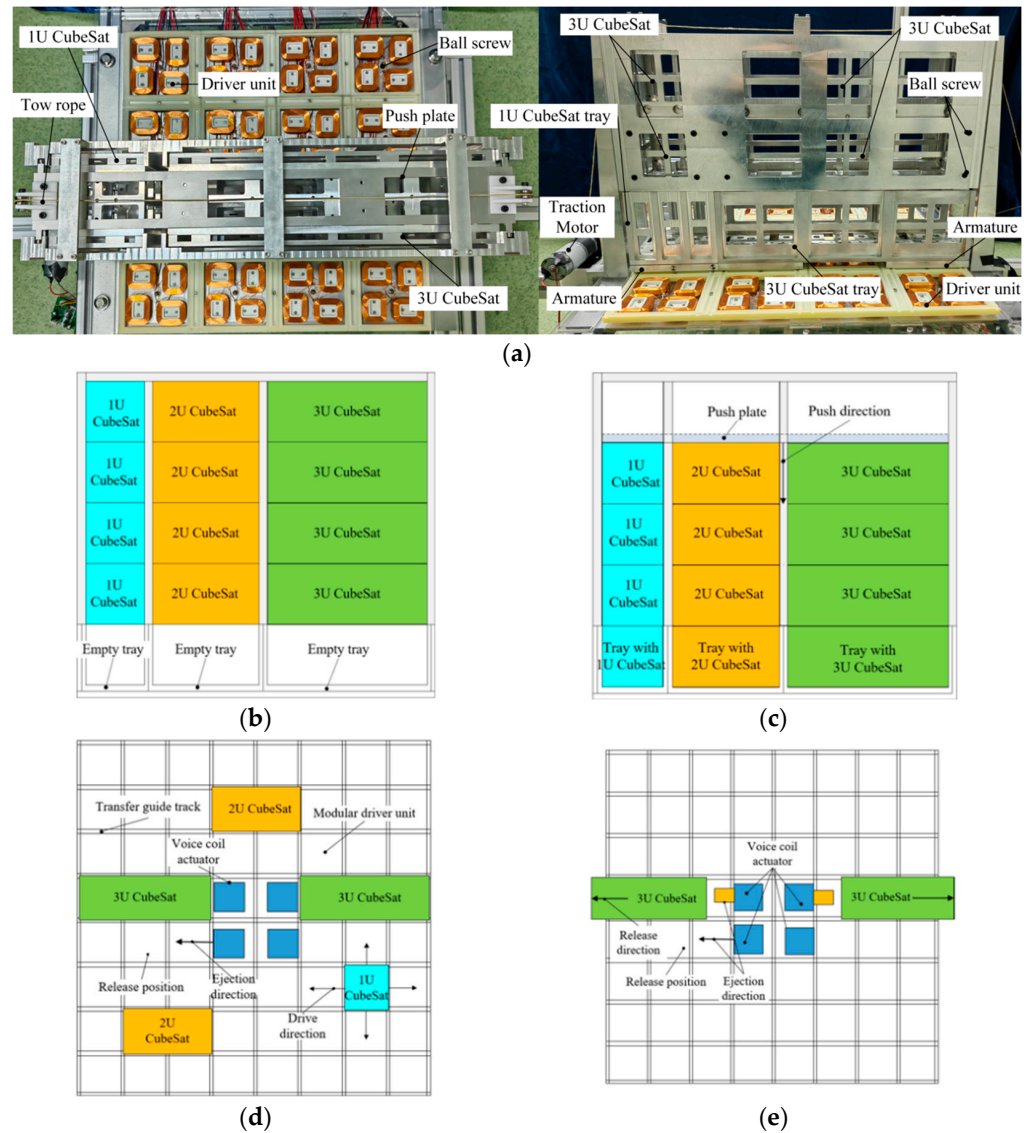


Figure 1. Schematic diagram of the in-orbit transfer and deployment system for large-scale CubeSats: (a) the physical diagram of the in-orbit transfer and deployment system for CubeSats; (b) initial state (front view); (c) pushing the CubeSats to the tray (front view); (d) transfer to the release window (vertical view); (e) ejection of CubeSats (vertical view).

2.2. The Grid-Based Method for the Transfer System

The main techniques for modeling the environment for path planning include geometric, grid-based, and topological methods. Due to its straightforward simplicity and ease of modeling, which matches well with the geometric characteristics of the CubeSat transfer platform, this paper utilizes the grid-based method. Based on the schematic diagram of the CubeSat two-dimensional transfer platform structure referenced in [15] (Figure 2), a 4×4 electromagnetic conveying platform is constructed. This setup includes several target CubeSats and moveable CubeSats. The start point of the target CubeSat is marked in green, while the endpoint is in red. The blue area indicates the CubeSat launch device, which is treated as an immovable barrier. The value of each cell on the platform corresponds to the movement cost for a CubeSat to that cell, initially set to zero, as depicted in Figure 3.

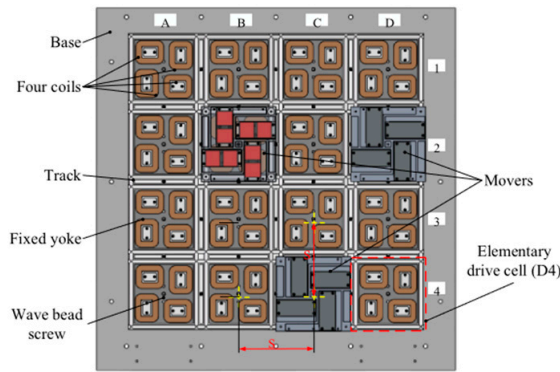


Figure 2. Schematic diagram of the two-dimensional transfer platform structure for CubeSats [15].

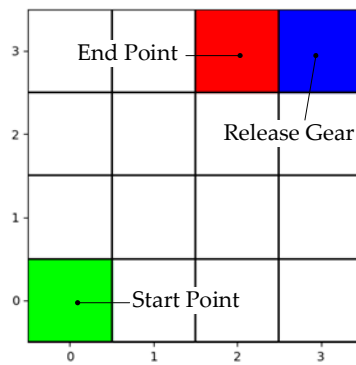


Figure 3. Initial environmental modeling diagram of the CubeSats transfer platform.

The coordinates (x, y) corresponding to the electromagnetic conveying platform can be represented as follows:

$$\begin{aligned} 0 \leq x < 4 \\ 0 \leq y < 4 \end{aligned} \tag{1}$$

3. Traditional A* Algorithm

3.1. Basic Principles

The A* algorithm establishes a cost function between the start point and the target point, giving the search a sense of purpose. The cost function of the traditional A* algorithm typically consists of two parts, formulated as follows:

$$f_0(n) = g_0(n) + h_0(n) \tag{2}$$

In the formula, $g_0(n)$ represents the cost for the CubeSat to move from the start point to the current grid n ; $h_0(n)$ represents the heuristic function for the CubeSat to move from the current grid n to the endpoint; $f_0(n)$ represents the cost function for the CubeSat to move from the start point to the endpoint.

In the traditional A* algorithm, considering the movement characteristics of the CubeSat on the electromagnetic conveying platform, which means the CubeSat can only move horizontally or vertically one grid at a time, the Manhattan distance is chosen as the heuristic function. The Manhattan distance represents the sum of the horizontal and vertical distances between two points, meaning that movement can only occur in four directions: up, down, left, and right within the grid. The formula is as follows:

$$g_0(n) = |x_n - x_s| + |y_n - y_s| \tag{3}$$

$$h_0(n) = |x_n - x_e| + |y_n - y_e| \tag{4}$$

In Equations (3) and (4), (x_n, y_n) represents the coordinates of the current cell n , (x_s, y_s) represents the coordinates of the starting point s , and (x_e, y_e) represents the coordinates of the endpoint e .

In the traditional A* algorithm, two lists are involved: the open list, containing the cost function values $f_0(n)$ for the four adjacent cells of the current cell, sorted in ascending order, and the closed list, encompassing all cells visited by the CubeSat. The path formed by connecting these cells in the closed list constitutes the final transfer path. Initially, the open list includes the coordinates of the start cell along with its corresponding $f_0(n)$ value, while the closed list starts empty.

3.2. Traditional A* Algorithm Logic

The traditional A* algorithm works as follows:

(1) Firstly, check if the open list is empty. If the open list is not empty, return the coordinates of the cell with the minimum $f_0(n)$ in the open list and add this coordinate to the closed list.

(2) Next, check if the current cell is the goal cell. If the current cell is the goal cell, the path is found. If the current cell is not the goal cell, search for adjacent reachable cells. If an adjacent reachable cell is not in the open list or the closed list, calculate the cost $f_0(n)$ for the adjacent reachable cell, add the coordinates and the $f_0(n)$ of the adjacent reachable cell to the open list, and set the current cell as the parent cell of the adjacent reachable cell.

(3) Repeat the above process. If the current cell is the goal cell, the optimal path is found, and the path is outputted. If the open list is empty, it indicates that no path is found.

The logic of the traditional A* algorithm is summarized as shown in Figure 4.

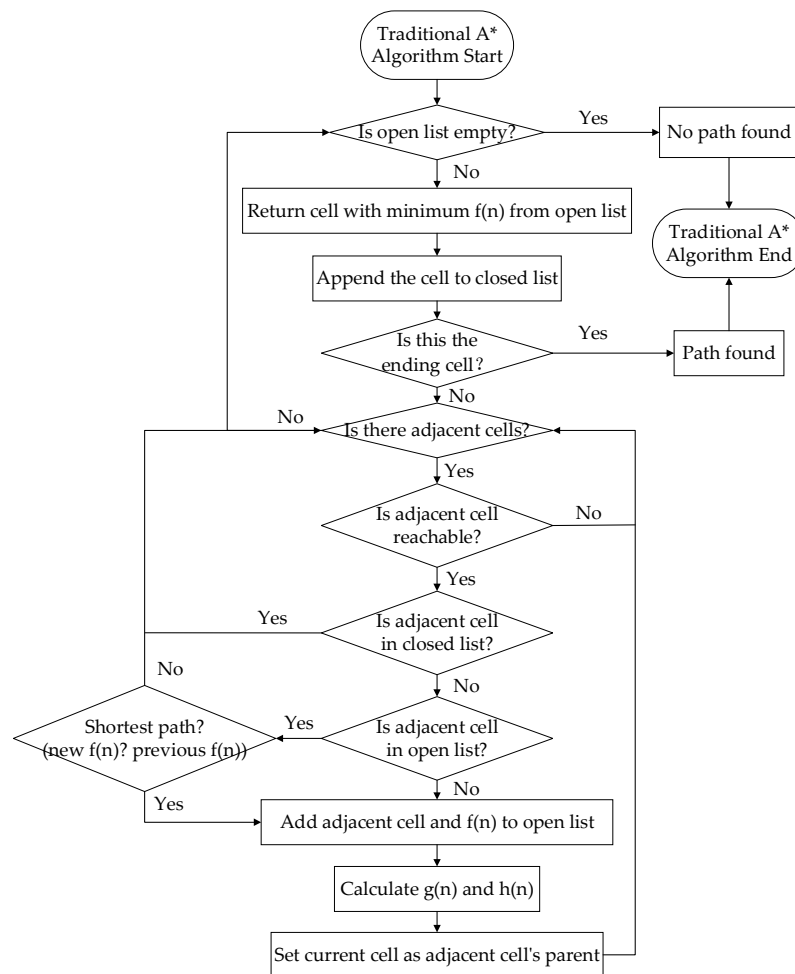


Figure 4. Flowchart of the traditional A* algorithm.

3.3. The Limitations of the Traditional A* Algorithm

The traditional A* algorithm is a heuristic search algorithm for finding the shortest path in a static road network, capable of quickly identifying the shortest path from a start point to a destination on a map. However, the traditional A* algorithm is not suitable for CubeSat in-orbit transfer path planning due to three reasons:

Firstly, the traditional A* algorithm's cost function does not align with the application requirements of CubeSat in-orbit transfer systems. According to the application requirements of CubeSat in-orbit transfer systems, the goal is to minimize the disturbance to the attitude of the electromagnetic conveying platform during CubeSat transfer while reducing the number of steps CubeSats take to reach their target positions as much as possible. However, the cost function of the traditional A* algorithm only focuses on minimizing path length and lacks cost estimation for the disturbance of the electromagnetic conveying platform's attitude caused by CubeSat transfer paths. Therefore, it is necessary to introduce a model for estimating the disturbance of the electromagnetic conveying platform's attitude and redesign the cost function of the improved A* algorithm to ensure that it meets the application requirements of CubeSat in-orbit transfer systems.

Secondly, the traditional A* algorithm cannot solve path-planning problems in dynamic road networks and is only suitable for planning paths in static road networks. However, the CubeSat in-orbit transfer system plans to utilize the transfer torque generated by the movement of other CubeSats to balance some of the transfer torque of the target CubeSat, aiming to minimize the disturbance to the attitude of the electromagnetic conveying platform during the transfer process. Therefore, the path planning problem for CubeSat in-orbit transfer is a multi-point, multi-objective path planning problem in a dynamic road network environment, which the traditional A* algorithm cannot solve.

Thirdly, the traditional A* algorithm fails to meet the efficiency requirements of multi-point, multi-objective path planning problems. The traditional A* algorithm stores all the information of the cells searched in the open list and arranges them in descending order. However, for a multi-point problem, each step corresponds to too many combinations of CubeSats, resulting in a large volume of data in the open list, which reduces the search efficiency.

In summary, the traditional A* algorithm cannot address the multi-point, multi-objective path planning challenges inherent in CubeSat in-orbit transfer. It falls short of meeting the application requirements, such as minimizing attitude interference and maximizing transfer efficiency in the CubeSat in-orbit transfer system. Therefore, it is imperative to improve the traditional A* algorithm.

4. Improved A* Algorithm

To accommodate the increasing future demand for CubeSats in orbit, the enhanced A* algorithm is pivotal for managing the simultaneous deployment of large batches of these satellites across a variety of applications, including routine operations, emergency services, and specialized scenarios such as space-based defense strategies. When instructed to deploy specific CubeSats, the electromagnetic transport system utilizes its built-in pusher to transfer them from storage to the transport platform. The enhanced A* algorithm then activates to identify the optimal path for moving the target CubeSats in conjunction with movable units. After the path is determined, the transport platform shifts the target CubeSats towards the launch window following this optimal route. The deployment concludes with the coil-type electromagnetic actuator ejecting and releasing the CubeSats into orbit, effectively executing the task of deploying numerous satellites simultaneously.

4.1. The Improved A* Algorithm Process Introduction

Considering the limitations of the traditional A* algorithm mentioned above, improvements should focus on establishing an attitude interference model, designing cost functions, introducing path coordination strategies, and optimizing the open list. The improved A* algorithm process is summarized in Figure 5, where the blue boxes repre-

sent the enhancements compared to the traditional A* algorithm. The CubeSats on the electromagnetic conveying platform are classified into two categories: target CubeSats and movable CubeSats. Target CubeSats are those that need to be transported to the CubeSat release window, while movable CubeSats refer to the other CubeSats on the platform, excluding the target CubeSats.

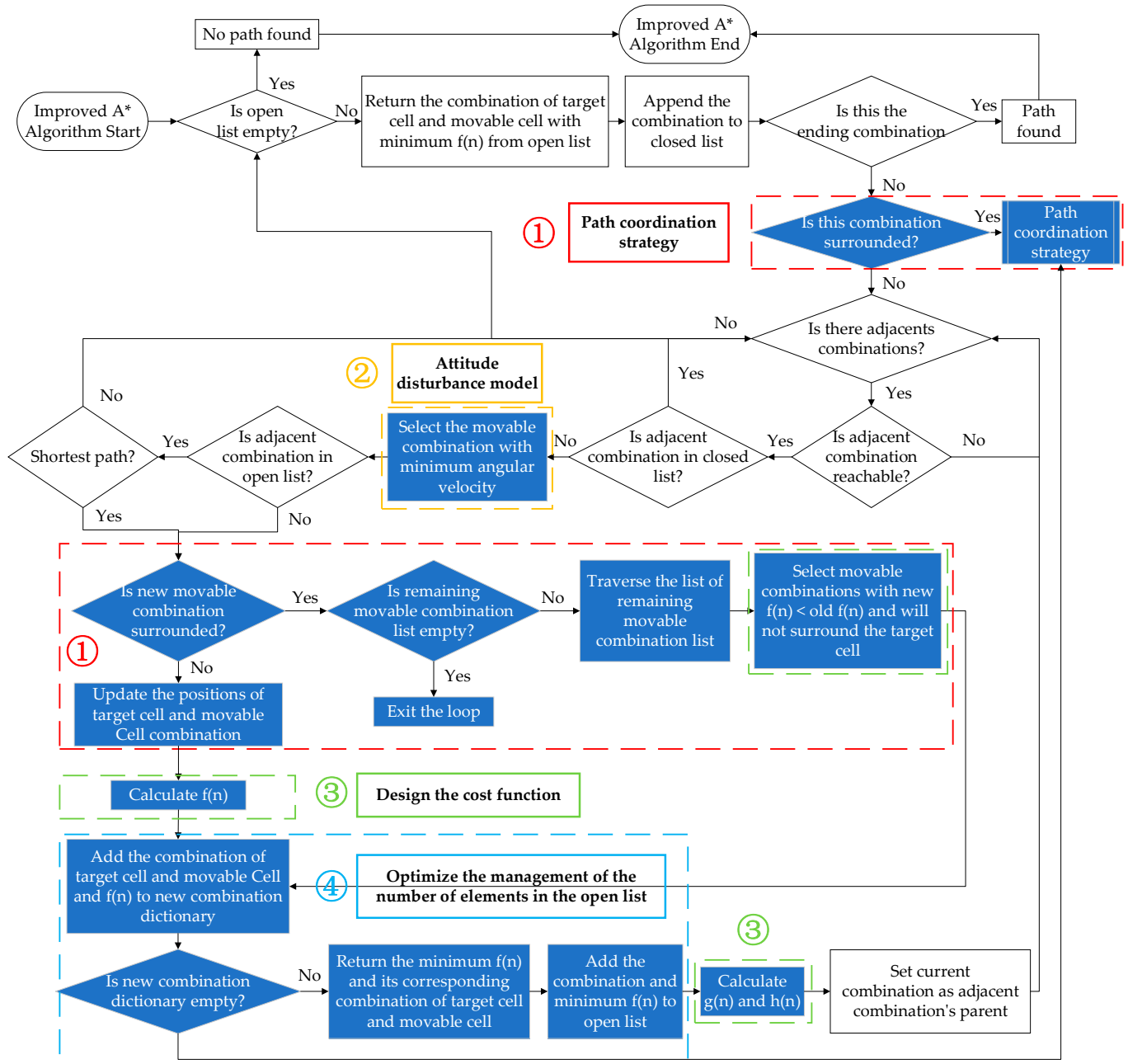


Figure 5. Improved A* algorithm flowchart.

Firstly, considering the capability of the CubeSat’s in-orbit electromagnetic transfer system to achieve large-scale deployment of payloads in orbit, there are typically a considerable number of CubeSats on the electromagnetic conveying platform, which can easily lead to congestion situations, thereby affecting the efficiency of CubeSat transfer. This article addresses this issue by introducing a check for whether the current combination of target CubeSats is congested before obtaining adjacent target CubeSat combinations. It proposes the introduction of a path coordination strategy to find alternative routes for congested

target CubeSats, ensuring that they can reach their intended release positions smoothly, as depicted in Figure 5①. If no feasible detour combination is found, the status of the target CubeSat combination is modified to unreachable to avoid unnecessary, redundant calculations, thereby enhancing the algorithm's operational efficiency and resource utilization.

Next, since CubeSat in-orbit transfer path planning involves a multi-point, multi-objective problem, before placing the target CubeSat combination into the open list, it is necessary to find the corresponding movable CubeSat combination. The newly established electromagnetic conveying platform attitude interference model can quantify the degree of CubeSat transfer process disturbance to the platform. This serves as the basis for filtering movable CubeSat combinations, ensuring that the torque generated by the transfer of movable CubeSat combinations can maximize the offset of the torque generated by the transfer of target CubeSats. This achieves the objective of minimizing the attitude interference of each step of CubeSat transfer to the electromagnetic conveying platform, as depicted in Figure 5②. Section 5 verifies the effectiveness of movable CubeSats combinations in reducing attitude disturbance of the electromagnetic conveying platform through comparative case studies.

If the new combination of target CubeSat and movable CubeSats is not in the open list (never visited before) or in the closed list but not part of the shortest path (previously visited but not the shortest path), before calculating the new cost function $f_1(n)$, a new judgment on whether the movable CubeSats will block the target CubeSat is added, as shown in Figure 5①. If the new movable CubeSats will block the target CubeSat, obtain the corresponding detour combination and add the transfer cost $f_1(n)$ of the detour combination to the transfer cost $f_1(n)$ of the movable CubeSats combination. Revisit the list of movable CubeSats combinations, filtering for the one with the minimum cost $f_1(n)$ to avoid falling into a local optimum and improve algorithm performance. If the new movable CubeSats do not block the target CubeSat, then calculate the transfer cost $f_1(n)$ for the new combination, as shown in Figure 5③. The transfer cost $f_1(n)$ needs to consider both the efficiency of CubeSat transfer and the degree of attitude interference caused by the transfer process on the electromagnetic conveying platform. To achieve this, a refined cost function should be devised, integrating the attitude interference model of the electromagnetic conveying platform into the A* algorithm's cost function. This entails setting separate coefficients k_h to represent CubeSat transfer efficiency and k_ω to denote the electromagnetic conveying platform attitude interference. By adjusting the ratio k_ω/k_h of these coefficients, the balance between the two factors in the cost function can be altered, thereby influencing CubeSat's in-orbit transfer path planning.

Finally, unlike the traditional A* algorithm, the improved A* algorithm does not directly add the coordinates of the new target CubeSat and movable CubeSat combination, along with the transfer cost $f_1(n)$, to the open list. Instead, they are first placed in a new combination dictionary. After traversing the adjacent reachable cells of the current target CubeSat and their corresponding movable CubeSat combinations, the improved A* algorithm returns the combination with the minimum transfer cost $f_1(n)$ from the new combination dictionary. This combination, along with its $f_1(n)$ value, is then added to the open list. This optimization effectively manages the number of elements in the open list, thereby enhancing the efficiency of the algorithm, as depicted in Figure 5④.

4.2. Establishing an Attitude Interference Model

The degree of attitude interference of CubeSats on the electromagnetic conveying platform during transfer can be measured by the torque generated by CubeSat transfer, the angular velocity and angular acceleration of the electromagnetic conveying platform, and the variation in the center of mass of the CubeSat in the in-orbit transfer system.

4.2.1. The Calculation of CubeSat Transfer Torque and Center of Mass Position

The movement of multiple CubeSats on the electromagnetic conveying platform can be approximated as a system of n mass points. The real-time center of gravity coordinates of

the CubeSats in-orbit electromagnetic transfer system can be calculated using the formula for the center of mass of a mass point system, as shown in Equation (5).

$$x_c = \frac{\sum_{i=1}^n m_i x_i}{\sum_{i=1}^n m_i}, y_c = \frac{\sum_{i=1}^n m_i y_i}{\sum_{i=1}^n m_i} \tag{5}$$

In Equation (5), (x_c, y_c) represents the center of mass coordinates of the electromagnetic conveying platform, m_i represents the mass of the i th CubeSat on the electromagnetic conveying platform, and (x_i, y_i) represents the coordinates of the i th CubeSat on the electromagnetic conveying platform.

According to reference [15], the movement of CubeSats on the electromagnetic conveying platform relies on electromagnetic force transfer provided by the transfer platform, where the transfer force for 1U, 2U, and 3U CubeSats can be approximately considered as F , $2F$, and $3F$, respectively. The degree of attitude disturbance to the electromagnetic conveying platform caused by CubeSat transfer can be measured by the magnitude of the torque exerted by the electromagnetic force on the central axis of the electromagnetic conveying platform during CubeSat transfer. The simplification of its dynamic model refers to the moment of spatial forces about the axis, measuring the change in the rotational state of an object around a certain axis. The calculation formula is shown in Equation (6). The magnitude of the torque is calculated according to Formula (6), and the sign is determined by the right-hand rule.

$$M_z(F) = \pm F \cdot d \tag{6}$$

In Equation (6), M_z represents the torque exerted by the CubeSat transfer force on the electromagnetic conveying platform, F represents the electromagnetic transfer force of the CubeSat, and d represents the distance from the center of mass of the electromagnetic conveying platform to the line of action of the CubeSat transfer force.

According to the movement of the CubeSat on the electromagnetic conveying platform, the torque magnitude and sign generated by the CubeSat’s movement in the right, down, left, and up directions are summarized in Table 1. In Table 1, (x, y) represents the centroid coordinates of the CubeSat, and (x_c, y_c) represents the centroid coordinates of the electromagnetic conveying platform.

Table 1. CubeSat movement torque table.

Movement Direction	Diagram	Magnitude of Torque	Polarity of Torque
right		$M_z = F \times (y_c - y)$	+: counterclockwise, -: clockwise
down		$M_z = F \times (x_c - x)$	
left		$M_z = F \times (y - y_c)$	
up		$M_z = F \times (x - x_c)$	

4.2.2. Angular Velocity and Angular Acceleration of the Electromagnetic Conveying Platform

The magnitude of the angular velocity and angular acceleration of the electromagnetic conveying platform can, to some extent, characterize the degree of attitude interference of the electromagnetic conveying platform. According to the differential equation of rigid body rotation about a fixed axis, it is known that the product of the moment of inertia of the rigid body about the rotation axis and the angular acceleration is equal to the algebraic sum of all the torques acting on the rigid body about the rotation axis. The formula is shown in (7).

$$\frac{dL_z}{dt} = J_z \frac{d\omega}{dt} = J_z \ddot{\varphi} = J_z \alpha = \sum M_z(F_i^e) \quad (7)$$

In Equation (7), J_z represents the moment of inertia of the electromagnetic conveying platform about its center axis, L_z denotes the angular momentum of the CubeSat transfer with respect to the center axis of the electromagnetic conveying platform, ω stands for the angular velocity of the electromagnetic conveying platform, and α represents the angular acceleration of the electromagnetic conveying platform.

From Equation (7), it can be observed that for different rigid bodies, assuming the same torque applied by the external force system to their axes, the larger the moment of inertia of the body about the axis, the smaller the angular acceleration α , and thus, the smaller the change in its rotational state; conversely, the smaller the moment of inertia of the body about the axis, the larger the angular acceleration α , and hence, the greater the change in its rotational state. Therefore, the moment of inertia of a rigid body is a measure of the rotational inertia of the body, just as mass is a measure of inertia for a particle.

According to the parallel axis theorem, the moment of inertia of a rigid body about any axis is equal to the moment of inertia about a parallel axis passing through the center of mass plus the product of the body's mass and the square of the distance between the two axes, as shown in Equation (8).

$$J_z = J_{zC} + Md^2 \quad (8)$$

In Formula (8), M represents the mass of the electromagnetic conveying platform, and d represents the distance between the current center of mass position (x_c, y_c) and the geometric center (x_o, y_o) of the electromagnetic conveying platform.

$$d = \sqrt{(x_c - x_o)^2 + (y_c - y_o)^2} \quad (9)$$

In Formula (8), J_{zC} represents the moment of inertia of the electromagnetic conveying platform about the axis passing through the center of mass, and J_z represents the moment of inertia of the electromagnetic conveying platform about the axis passing through the geometric center of the electromagnetic conveying platform. According to the relevant technical manual, J_z can be expressed as follows:

$$J_z = \frac{M}{12} (a^2 + b^2) \quad (10)$$

In Formula (10), M represents the mass of the electromagnetic conveying platform, and a and b , respectively, represent the length and width of the electromagnetic conveying platform.

Therefore, the angular acceleration of the electromagnetic conveying platform can be expressed as follows:

$$\alpha = \frac{\sum M_z(F_i^e)}{\frac{M}{12}(a^2 + b^2) - M[(x_c - x_o)^2 + (y_c - y_o)^2]} \quad (11)$$

Thus, the angular velocity of the electromagnetic conveying platform can be expressed as follows:

$$\omega = \int \alpha dt = \int \frac{\sum M_z(F_i^e)}{\frac{M}{12}(a^2 + b^2) - M[(x_c - x_o)^2 + (y_c - y_o)^2]} dt \quad (12)$$

Combining the analysis of the application scenarios of CubeSats in-orbit electromagnetic transfer system, it can be inferred that the maximum angular velocity of the electromagnetic conveying platform during the transfer process and the final angular velocity after transfer play a crucial role in the attitude stability of the CubeSats in-orbit electromagnetic transfer system.

$$P_1(n) = k_\omega \omega_1(n) = k_\omega \int_{i=1}^n \frac{\sum M_z(F_i^e)}{\frac{M}{12}(a^2 + b^2) - M[(x_c - x_o)^2 + (y_c - y_o)^2]} dt \quad (13)$$

In Equation (13), $P_1(n)$ represents the attitude disturbance model of the electromagnetic conveying platform, $\omega_1(n)$ denotes the real-time angular velocity of the electromagnetic conveying platform, and k_ω represents the weight coefficient corresponding to the cost of the attitude disturbance level of the electromagnetic conveying platform.

4.3. Design the Cost Function

The cost function can be expressed as a comprehensive consideration of both the disturbance level of the CubeSat in-orbit electromagnetic transfer system to the attitude of the electromagnetic conveying platform and the efficiency of the CubeSat in-orbit transfer.

$$f_1(n) = k_h[g_1(n) + h_1(n)] + P_1(n) = k_h[g_1(n) + h_1(n)] + k_\omega \omega_1(n) \quad (14)$$

In Equation (14), k_h represents the weighting coefficient of the cost associated with the efficiency of CubeSat in-orbit transfer. By adjusting the ratio between k_h and k_ω , the paper can change how much CubeSat's transfer system prioritizes efficiency versus minimizing attitude disturbance to the electromagnetic conveying platform in the overall transfer cost. Increasing k_h favors finding the shortest transfer path for CubeSat, somewhat overlooking the potential disturbance to the electromagnetic conveying platform's attitude caused by the path. Conversely, raising k_ω prompts the system to prioritize minimizing attitude disturbance to the electromagnetic conveying platform when choosing a path, potentially overlooking CubeSat transfer efficiency and leading to locally optimal solutions. The function $g_1(n)$ represents the Manhattan distance for a CubeSat to move from the starting point (x_s, y_s) to the current cell (x_n, y_n) . It can be expressed as:

$$g_1(n) = |x_n - x_s| + |y_n - y_s| \quad (15)$$

$h_1(n)$ represents the heuristic function for the CubeSat to move from the current position (x_n, y_n) to the destination (x_e, y_e) , and it can be expressed as follows:

$$h_1(n) = |x_n - x_e| + |y_n - y_e| \quad (16)$$

Based on the cost function, the initial conditions for the improved A* algorithm for CubeSat's in-orbit transfer path planning are designed, as shown in Table 2.

Table 2. Example of initial conditions for CubeSat’s in-orbit electromagnetic transfer system.

Example Number	Target CubeSat					Movable CubeSats			
	Name	Type	Start Point	Endpoint	Color	Name	Type	Initial Coordinates	Color
1	C1	1U	(0, 0)	(2, 3)	Green	A1	2U	(1.5, 1)	Yellow
2	C1	1U	(0, 0)	(2, 3)	Green	A1	2U	(1.5, 1)	Yellow
						A2	1U	(3, 0)	Orange
3	C1	1U	(0, 0)	(2, 3)	Green	A1	2U	(1.5, 1)	Yellow
						A2	1U	(3, 0)	Orange
						A3	3U	(2, 2)	Blood orange

The release device is located at (3,3); it does not move and can be considered as the wall.

The initial conditions for each example are shown in Figure 6.

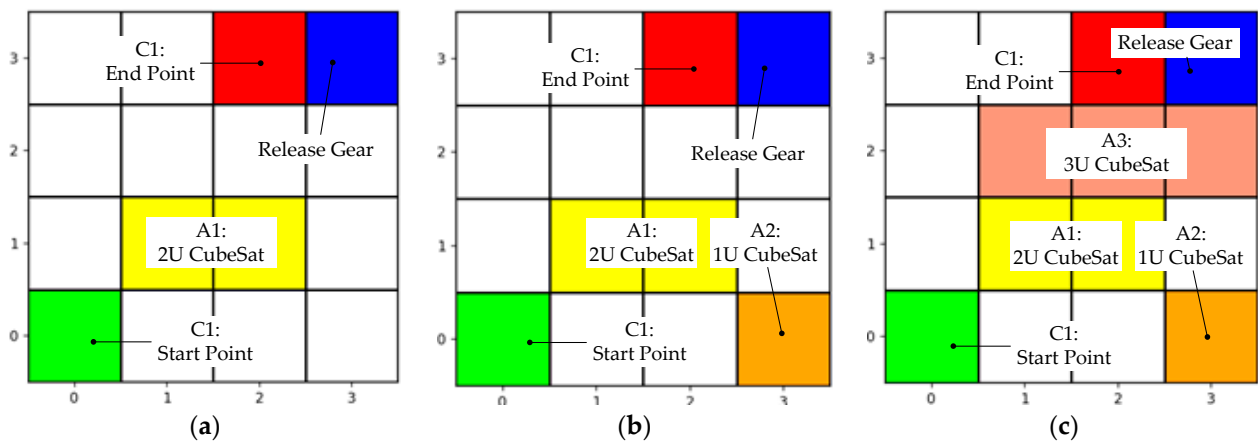


Figure 6. Initial situation diagram of the CubeSat’s in-orbit transfer system path planning example: (a) initial condition diagram for Example 1; (b) initial condition diagram for Example 2; (c) initial condition diagram for Example 3.

The results of the algorithm’s operational testing are shown in Figure 7. In Figure 7, arrows point to the current cell’s parent.

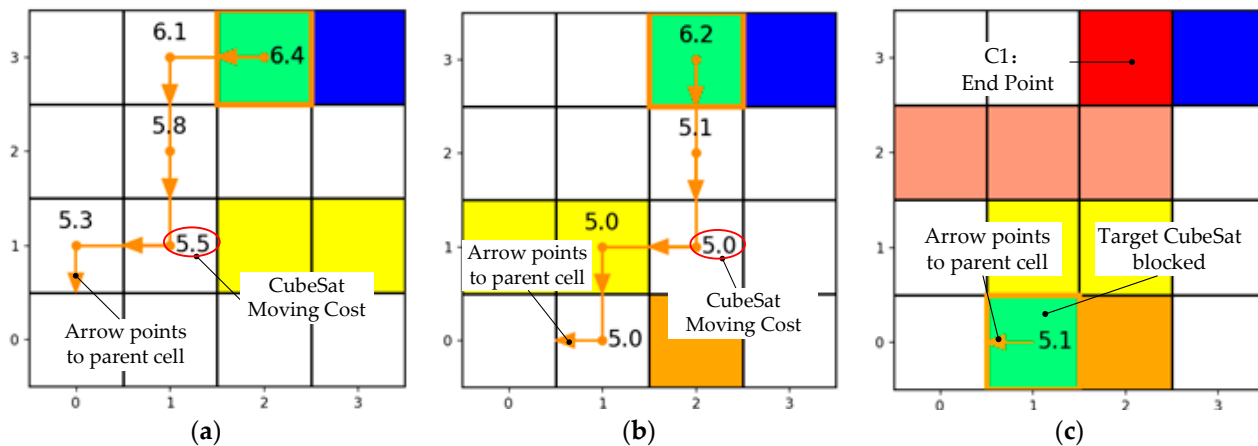


Figure 7. Test results of the path planning algorithm for the CubeSat’s in-orbit transfer system: (a) algorithm test results for Example 1; (b) algorithm test results for Example 2; (c) algorithm test results for Example 3.

From Figure 7c, it can be observed that the CubeSat shown in Example 3 is surrounded by other CubeSats during the transfer process, resulting in the interruption of the algorithm and the failure to reach the destination. Analysis indicates that as the number of CubeSats on the electromagnetic conveying platform increases, it is inevitable that situations where the target CubeSat is surrounded by other CubeSats will occur. Therefore, introducing the path coordination strategy to address this situation is necessary.

4.4. The Path Coordination Strategy

The application scenarios for path coordination strategies in CubeSat deployment can broadly be categorized into two types: those where the deployment sequence is known and those where it is unknown. In the first scenario, where the deployment sequence of CubeSats is known, such as in routine deployment tasks, the CubeSats' in-orbit electromagnetic transfer system pushes entire layers of CubeSats simultaneously to the transport platform. This approach means that both target and movable CubeSats are moved to the platform together. However, as the number of CubeSats on the platform increases, issues such as path congestion inevitably arise. Path coordination strategies are then crucial for ensuring that target CubeSats can efficiently reach the launch window without disruptions. In the second scenario, where the deployment sequence is unknown, the role of path coordination strategies becomes even more critical. These strategies prevent the transport process from getting bogged down in local optima. As shown in the operational logic of the improved A* algorithm (illustrated in Figure 5), before implementing a transport plan that offers the lowest transport cost for the target CubeSat and movable CubeSat at that step, it is vital to assess whether the plan might cause path blockages. If potential blockages are identified, path coordination strategies are employed to devise alternative plans that circumvent these issues. This proactive integration of path coordination strategies into the improved A* algorithm helps to avoid local optima and significantly boosts the efficiency of CubeSat in-orbit transportation.

The path coordination strategy mainly consists of four levels. Firstly, it checks whether the target CubeSats are blocked. If the current target CubeSats are blocked, it then identifies which movable CubeSat is blocking it and subsequently obtains the path coordination combination corresponding to the current target CubeSats' associated movable CubeSats, which is process 1. Next, it should be determined whether the path coordination combination of the target CubeSats and movable CubeSats will block the path. If the path coordination combination of the movable CubeSats does not block the path, it indicates that the combination is feasible; otherwise, it indicates that the combination is not feasible. If a feasible path coordination combination cannot be found, indicating that Process 1 is not feasible, it means that the position of the movable CubeSats combination corresponding to the current target CubeSats needs to be changed, which is Process 2. If the current target CubeSats are still blocked after changing the position of the movable CubeSats, the path coordination combination corresponding to the changed position of the movable CubeSats is obtained, which is Process 3. If no path coordination combination is found corresponding to the changed position of the movable CubeSats, it indicates that none of the movable CubeSats combinations corresponding to the current target star are feasible. Therefore, it is necessary to change the position of the movable CubeSats corresponding to the target CubeSat combination's parent, which is Process 4. The flowchart of the path coordination strategy is shown in Figure 8.

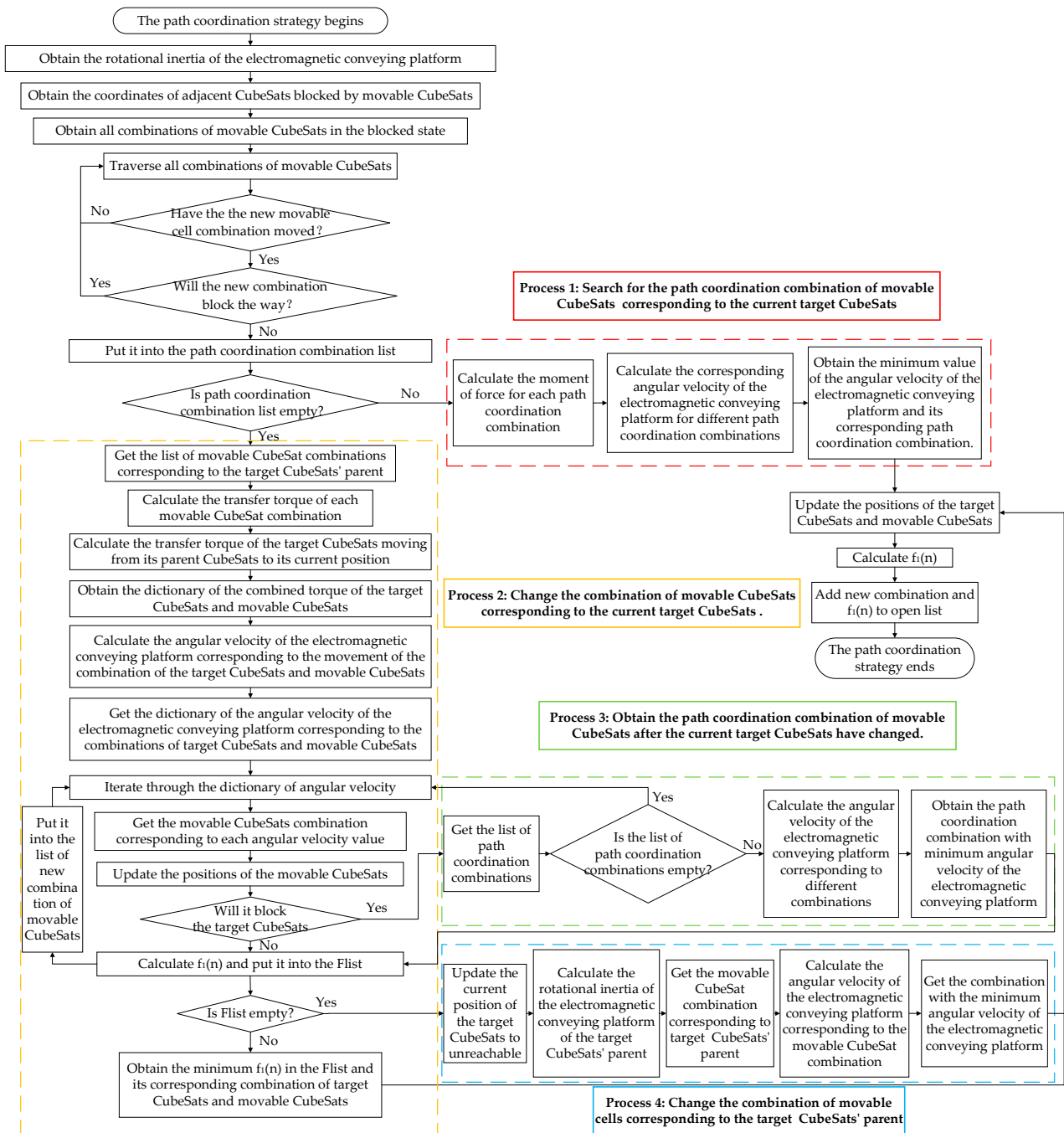


Figure 8. Flowchart of the path coordination strategy.

The key points of the path coordination strategy lie in how to determine if the target CubeSat combination is blocked, by whom, and whether the new combination obstructs the path. The specific solution is as follows:

(1) Determine if the target CubeSat combination is blocked: Firstly, obtain the coordinates and accessibility of the adjacent cells from the current position of the target CubeSat combination. If all adjacent cells are inaccessible, then the target CubeSat combination is considered blocked; otherwise, if at least one adjacent cell is accessible, then the target CubeSat combination is not blocked.

(2) Determine which movable CubeSat blocks the target CubeSat combination: Since the target CubeSat combination’s transfer strategy involves traversing adjacent cell coordinates, moving only one step at a time without backtracking, the adjacent cell coordinates

of the target CubeSat combination does not include cases where all four directions (right, down, left, up) have been visited. In other words, if all adjacent cell coordinates are already in the closed list, it implies that the target CubeSat combination is blocked by another CubeSat. Therefore, the key to this problem lies in determining which movable CubeSat blocks the target CubeSat combination. Firstly, obtain the coordinates of the adjacent cells of the target CubeSat combination and remove the visited coordinates. Obtain the current movable CubeSat coordinate dictionary, where the movable CubeSat name serves as the key and the list of occupied cell coordinates serves as the value. Traverse the coordinates of the adjacent cells of the target CubeSat combination and check if they are in the movable CubeSat coordinate dictionary. If found, return the corresponding key of the coordinate, which represents the movable CubeSat name, indicating that the target CubeSat combination is blocked by this movable CubeSat.

(3) Determine whether the given combination of the target CubeSats and movable CubeSats will block the path: Firstly, obtain the coordinates of the adjacent cells of the target CubeSats and remove the coordinates that have been visited. Then, obtain the list of cell coordinates occupied by the movable CubeSat combination. Finally, traverse the adjacent cell coordinates of the target CubeSats. If there are adjacent cell coordinates that are not in the list of movable CubeSat coordinates, it indicates that this combination will not block the path. Conversely, if all adjacent cell coordinates are in the list of movable CubeSat coordinates, it indicates that this combination will block the path.

Following the implementation of the path coordination strategy, the test results for Example 3 are depicted in Figure 9 (with $k_w/k_h = 1$).

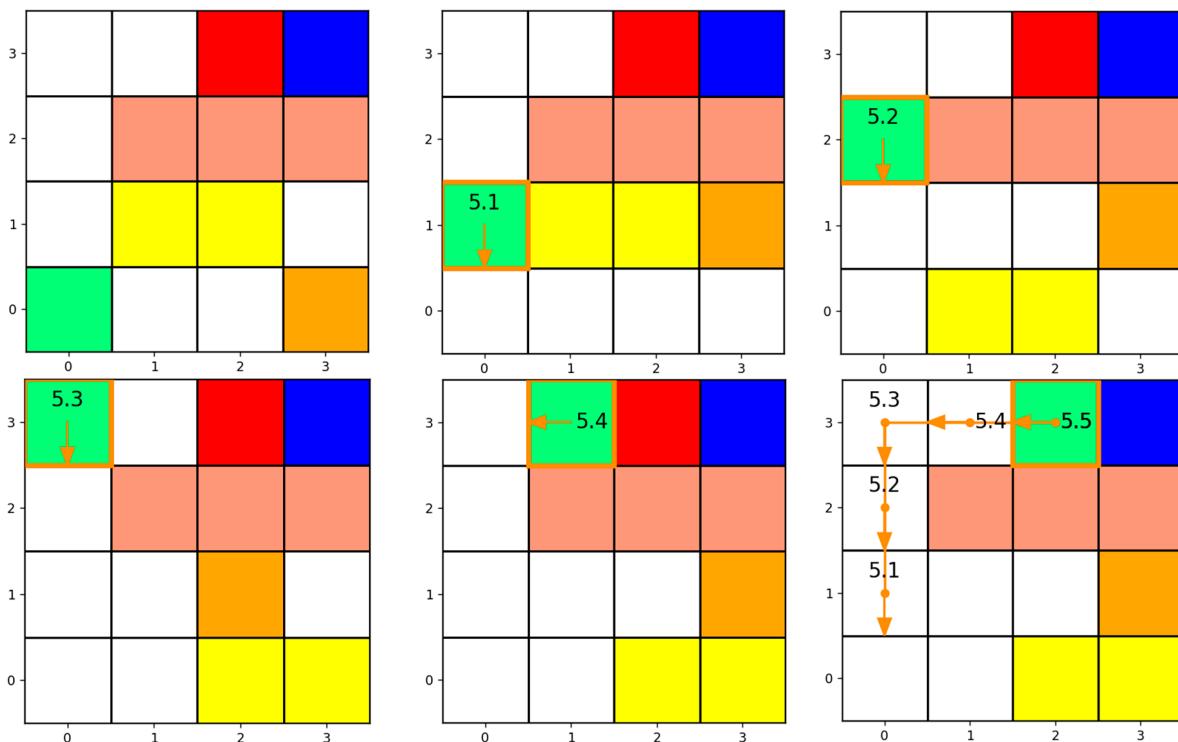


Figure 9. Transfer path for Example 3 after implementation of path coordination strategy.

4.5. Optimize the Open List

During the algorithm testing process, it was observed that as the number of CubeSats increased, the algorithm runtime also increased, failing to meet the requirement for quick response. Optimization of the algorithm is necessary. During the execution of the traditional A* algorithm, expanding a node involves computing the transfer cost $f_0(n)$ for all adjacent nodes and sorting them in the open list in descending order. Due to the numerous combinations of target CubeSats and movable CubeSats, the size of the open list is large.

Consequently, the computation time required to return the combination with the minimum $f_0(n)$ value from the open list also increases, thus reducing the speed of open list expansion. In the improved A* algorithm, this paper optimizes the management of the number of nodes in the open list by introducing a new combination dictionary. The positions and corresponding transfer costs $f_1(n)$ obtained from traversing the target CubeSat combinations at each step are first placed into the new combination dictionary. This allows for the comparison of $f_1(n)$ values before placing them into the open list, ensuring that only the combination with the minimum $f_1(n)$ and its corresponding $f_1(n)$ are placed into the open list. This reduces the number of nodes in the open list and effectively improves the efficiency of the algorithm.

5. Test of the Improved A* Algorithm

To highlight the advantages of using the improved A* algorithm for optimizing transfer paths in reducing disturbances to the electromagnetic conveying platform’s attitude, this paper presents a comparative analysis. This analysis focuses on how the inclusion of movable CubeSats affects the stability of the platform during the transfer of target CubeSats. The paper explores two case studies: Case Study 1, which involves only target CubeSats on the transport platform, and Case Study 2, which replicates the setup of Case Study 1 but includes a specific number of movable CubeSats. By comparing the impact of the optimal transfer paths from both cases on the platform’s attitude disturbance, the paper demonstrates the effectiveness of the improved A* algorithm in maintaining platform stability.

5.1. Design Test Cases

Considering the physical and structural parameters of the CubeSats in-orbit electromagnetic transfer system, the size of the electromagnetic conveying platform has been expanded to an 8×8 configuration. In Case 1, only four target CubeSats (C1, C2, C3, and C4) are placed on the platform, whereas Case 2 also includes five movable CubeSats (A1, A2, A3, A4, and A5). Detailed parameters for these configurations are listed in Table 3. The initial setups for Case 1 and Case 2 are depicted in Figure 10.

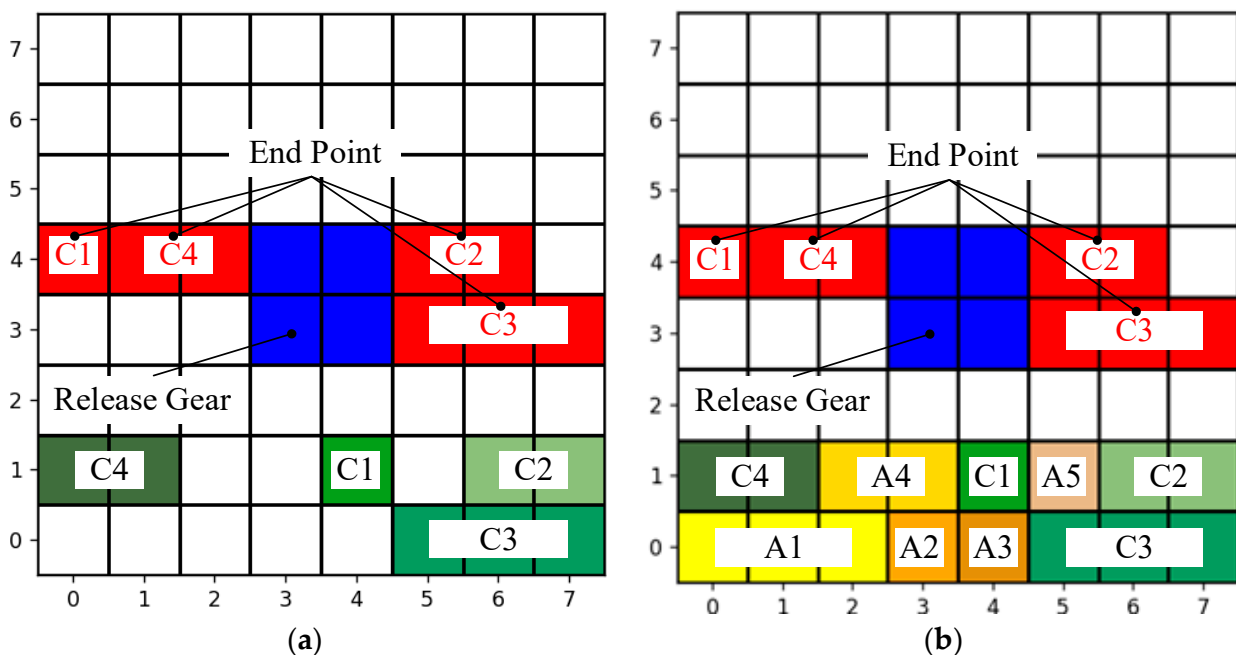


Figure 10. Initial situation of the test case for the improved A* algorithm: (a) Case 1; (b) Case 2.

Table 3. Initial conditions for testing the improved A* algorithm in CubeSat’s in-orbit electromagnetic transfer system.

Target CubeSat					Movable CubeSats			
Name	Type	Start Point	Endpoint	Color	Name	Type	Initial Coordinates	Color
C1	1U	(4, 1)	(0, 4)	Forest Green	A1	3U	(1, 0)	Yellow
C2	2U	(6.5, 1)	(5.5, 4)	Sage Green	A2	1U	(3, 0)	Orange
C3	3U	(6, 0)	(6, 3)	Fern Green	A3	1U	(4, 0)	Goldenrod
C4	2U	(0.5, 1)	(1.5, 4)	Camouflage Green	A4	2U	(2.5, 1)	Gold
					A5	1U	(5, 1)	Burlywood

The release device is located at the geometric center of the electromagnetic conveying platform, occupying a total of 4 grid cells, namely (3,3), (3,4), (4,3), and (4,4), marked in blue. The release device remains stationary and can be treated as the wall.

5.2. Improved A* Algorithm Test Results

Based on the initial conditions described, the improved A* algorithm was tested to optimize the selection of target and movable CubeSats using the cost function $f_1(n)$. Here, k_ω/k_h plays a crucial role as it represents the ratio between the degree of attitude disturbance caused by the CubeSat transfer to the electromagnetic conveying platform and the efficiency of the CubeSat transfer path, measured by the number of steps. These performance indicators proportionally influence the CubeSat on-orbit transfer path scheme.

The goal of this study is to find the most suitable in-orbit transfer paths for CubeSats that minimize attitude disturbances to the electromagnetic conveying platform while also reducing the number of movement steps needed for CubeSats to reach their designated positions. The paper evaluated the ratios of k_ω/k_h from 0 to 50, generating 51 potential transfer scenarios across two case studies. The ratio k_ω/k_h impacts the transfer cost $f_1(n)$ for each path segment, influencing path selection at each step. If an increase in k_ω/k_h does not adequately compensate for the efficiency cost differences among transfer paths, the CubeSat transfer plan remains unchanged, which leads to duplicate scenarios among the 51 paths. After removing duplicates, the analysis yielded one feasible transfer path for the first case study and seven for the second. Detailed parameters for these scenarios in the second case study are listed in Table 4.

Table 4. Parameters of transfer path schemes for CubeSats in-orbit for Case 2.

Scheme Number	k_ω/k_h	Steps	Maximum Transfer Torque/Nm	Final Angular Velocity /rad·s ⁻¹	Final Angular Acceleration/ rad·s ⁻²
1	0	35	109.9998	−0.0178	0.0171
2	0.8	45	50.6619	−0.0040	−0.0019
3	1.8	73	64.0225	−0.0034	0.0011
4	2.3	38	64.1408	−0.0785	0.0050
5	2.7	47	50.6470	−0.0026	0.0009
6	3.0	81	72.0000	−0.0231	−0.0576
7	3.8	40	50.6619	−0.0069	0.0000

Considering both the efficiency of CubeSat’s transfer and the degree of disturbance to the electromagnetic conveying platform caused by this transfer, Scheme 5 is chosen as the ultimate transfer path scheme for Case 2 study.

In Scheme 5, with $k_\omega/k_h = 2.7$, Case 2’s transfer path includes 47 steps to reach the designated launch area and is completed in 14.7 s of algorithm operation, as depicted in Figure 11. To provide a clearer visual representation of this complex path, the steps are detailed in Figure 12. This paper sets the parameters for each cell on the electromagnetic conveying platform, noting the side length as $l = 10$ cm, and establishes the average transfer speed of CubeSats as $v = 0.2$ m/s. Given the movement characteristics of CubeSats on this platform, they are limited to moving horizontally or vertically, one cell at a time. Therefore,

the total distance $s = 1 \times \text{path}$ that CubeSats travel during transport and the necessary time for transport can be determined using Equation (17). In Case 2, the transfer path consists of 47 steps. By inputting this value into Equation (17), the total time needed for the transport in Case 2 is 23.5 s.

$$t = \frac{s}{v} = \frac{l \times \text{path}}{v} \tag{17}$$

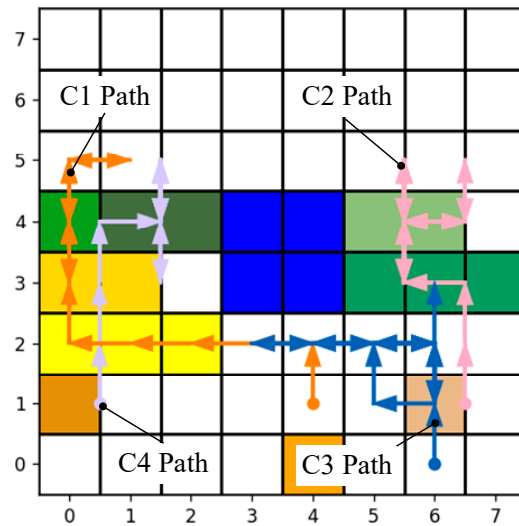


Figure 11. Improved A* algorithm Test Case 2 transfer path (Scheme 5).

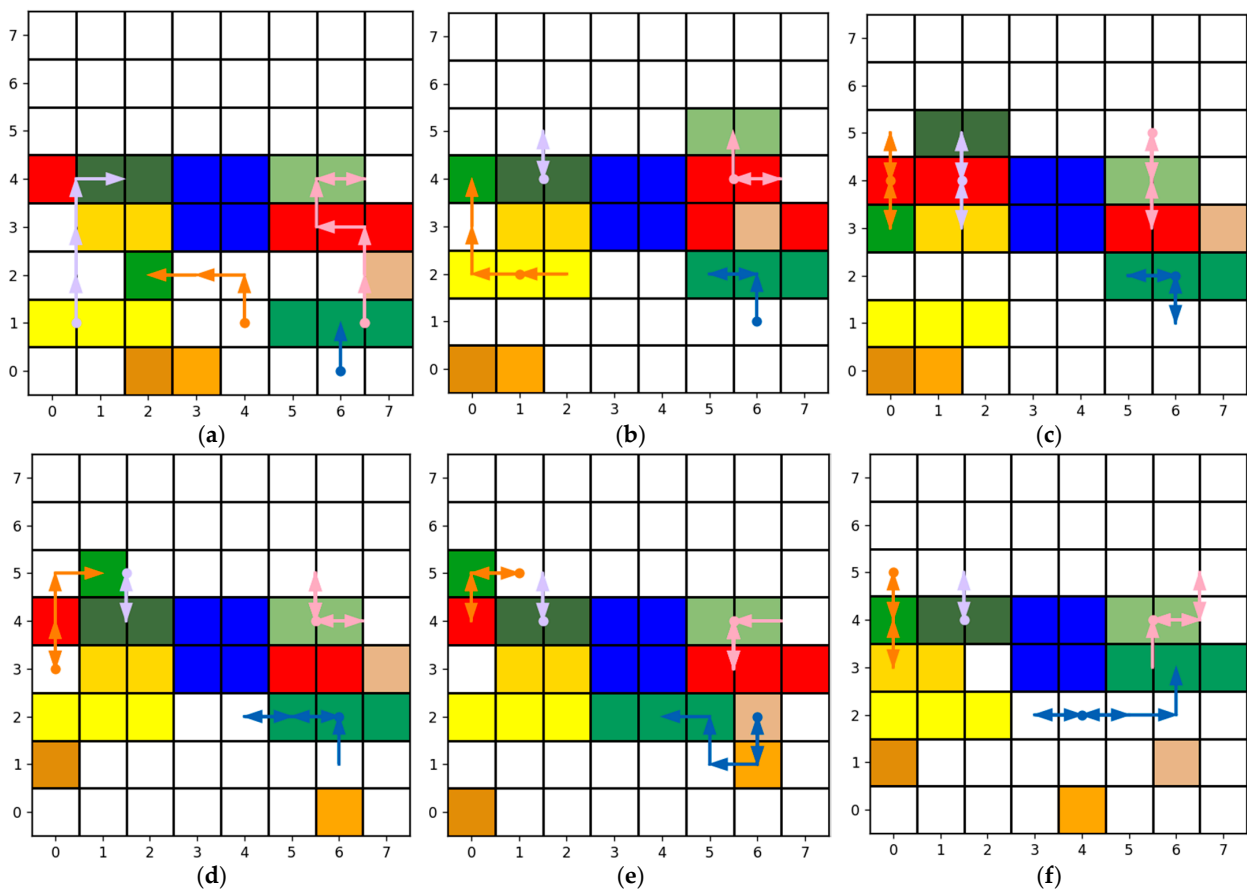


Figure 12. Stepwise representation of the improved A* algorithm Case 2 transfer path (Scheme 5): (a) steps 1~8; (b) steps 9~16; (c) steps 17~24; (d) steps 25~32; (e) steps 33~40; (f) steps 41~47.

The curves for the angular velocity and angular acceleration of the electromagnetic conveying platform are depicted in Figure 13. During the transfer process of the target CubeSats, the maximum torque experienced by the electromagnetic conveying platform is approximately 50.6740 Nm, occurring around the 12th step of the target CubeSats transfer path. Upon comparison with Figure 14, it becomes apparent that the peak angular velocity and maximum angular acceleration of the electromagnetic conveying platform similarly manifest near the 12th step of the transfer path. The analysis suggests that the substantial combined torque arising from the movement of the target CubeSats and the mobile CubeSats combination at the 12th step leads to an escalation in both the angular velocity and angular acceleration of the electromagnetic conveying platform, aligning with the qualitative analysis outcomes of the electromagnetic conveying platform's attitude disturbance model. The final angular acceleration of the electromagnetic conveying platform is $0.0009 \text{ rad}\cdot\text{s}^{-2}$, and the final angular velocity is $-0.0026 \text{ rad}\cdot\text{s}^{-1}$. Throughout the transfer process, the maximum angular velocity of the electromagnetic conveying platform is approximately $-0.029 \text{ rad}\cdot\text{s}^{-1}$. Following the 23rd step, the electromagnetic conveying platform experiences consistent transfer torque. The curves depicting the angular velocity and angular acceleration of the electromagnetic conveying platform remain steady, with final values relatively small. This stability indicates that the electromagnetic conveying platform maintains a consistent attitude. Moreover, the number of transfer steps is moderate. Therefore, for the Case 2, Scheme 5 is selected as the final transfer path.

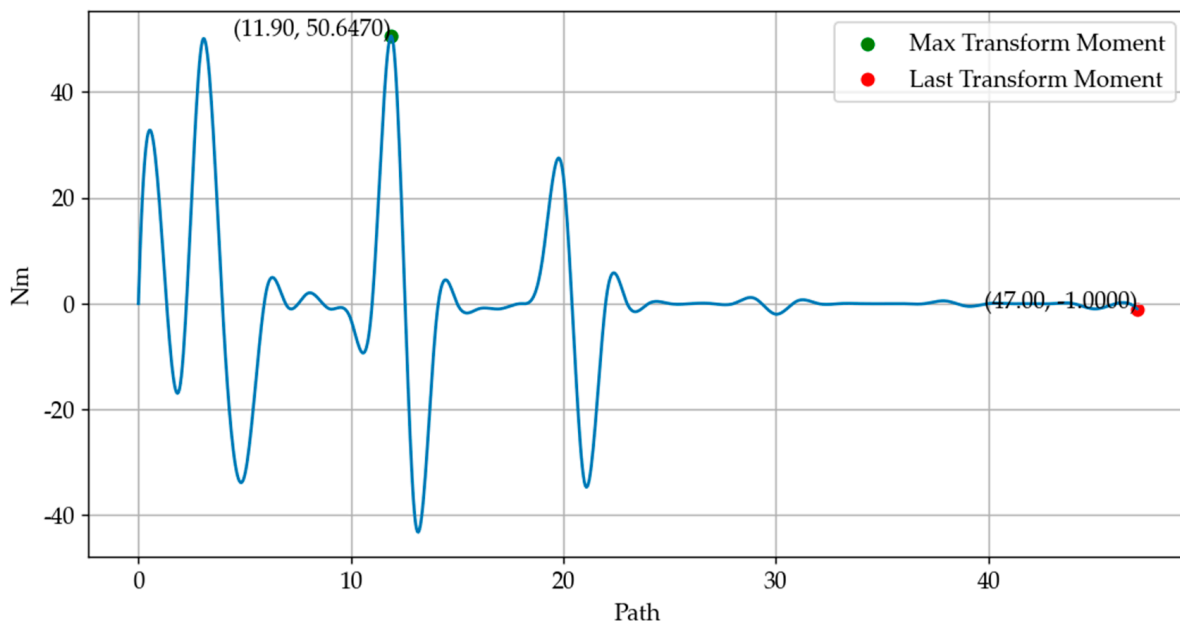


Figure 13. Improved A* algorithm Test Case 2 transfer torque graph (Scheme 5).

In Case 1, a single feasible transfer path was identified. Utilizing the improved A* algorithm, the target CubeSats were successfully navigated to the launch window in eight steps, with the algorithm completing in roughly 2.11 s, as depicted in Figure 15. During this process, the electromagnetic conveying platform exhibited a torque curve, shown in Figure 16, where the maximum torque reached 102.5814 Nm and concluded at -30 Nm . A comparison of the torque profiles between Case 1 and Case 2, illustrated in Figure 13, shows that both the maximum and final torques in Case 1 are substantially higher than those in Case 2. Additionally, the torque curve for Case 1 exhibits significant fluctuations, indicating pronounced disturbances to the platform's attitude. Further examination of the dynamics of the platform in Case 1, presented in Figure 17, shows the maximum angular velocity was $-0.2253 \text{ rad}\cdot\text{s}^{-1}$, and the final angular velocity was $-0.2106 \text{ rad}\cdot\text{s}^{-1}$. In comparison, the data from Case 2, shown in Figure 14, reveal that the maximum angular velocity in

Case 1 is about seven times higher and the final angular velocity approximately 77 times higher than those in Case 2. Moreover, while Case 2 displays stable angular velocities and accelerations toward the end of the transfer, Case 1 experiences ongoing significant fluctuations. This analysis highlights the essential role of movable CubeSats in balancing the torque generated by the target CubeSats, which crucially contributes to maintaining the stability of the platform’s attitude.

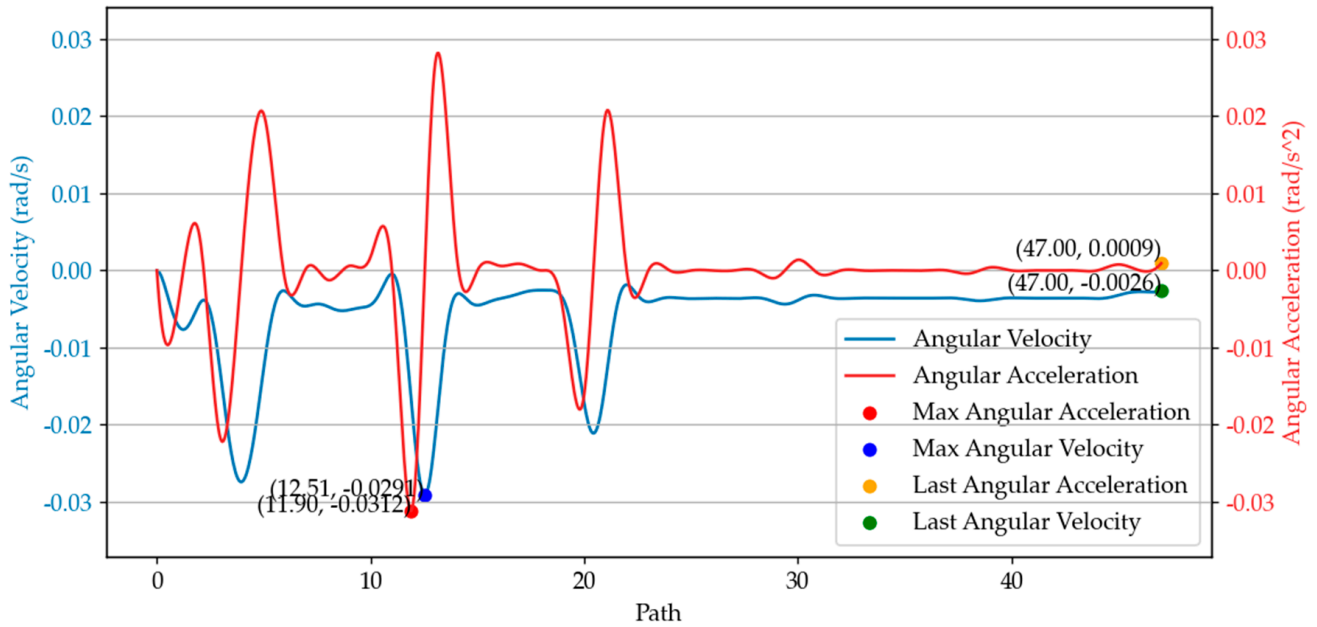


Figure 14. Curve graph of angular velocity and angular acceleration of the electromagnetic conveying platform in the improved A* algorithm test case 2 (Scheme 5).

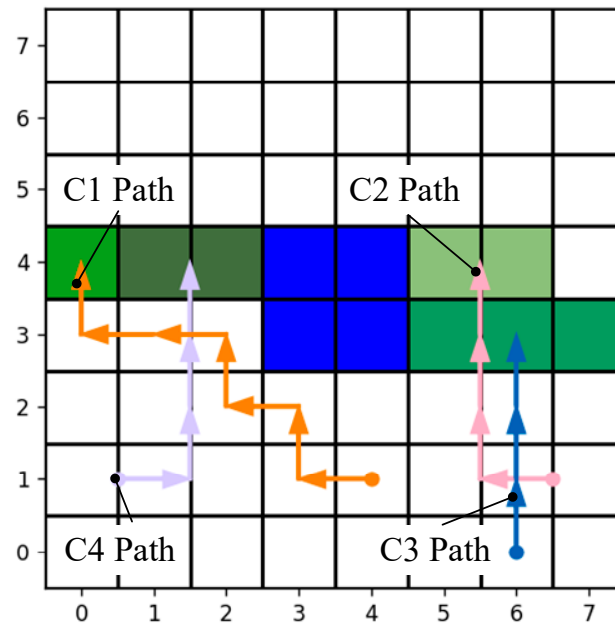


Figure 15. Improved A* algorithm Test Case 1 transfer path.

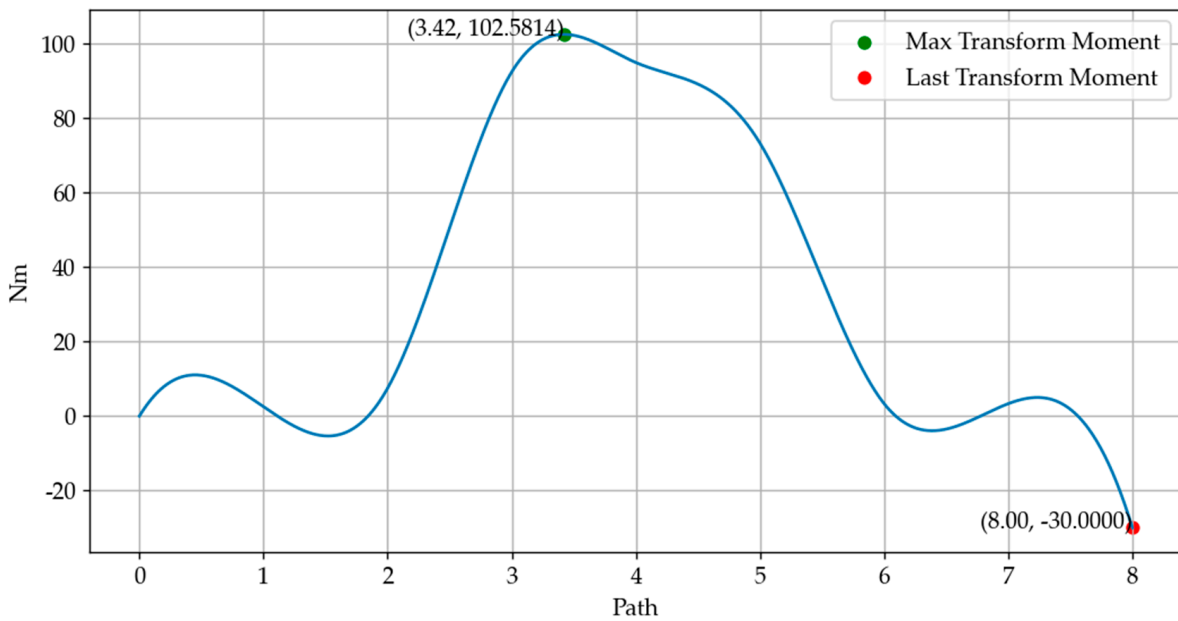


Figure 16. Improved A* algorithm Test Case 1 transfer torque graph.

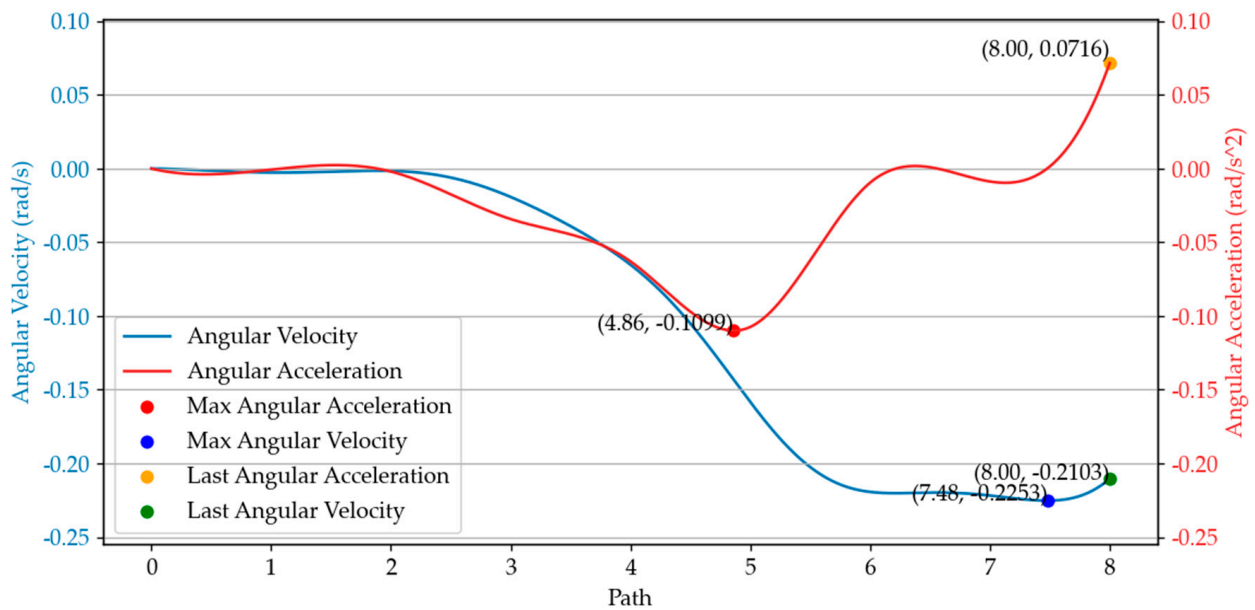


Figure 17. Curve graph of angular velocity and angular acceleration of the electromagnetic conveying platform in the improved A* algorithm Test Case 1.

6. Conclusions

The paper introduces an improved A* algorithm tailored for path planning within the CubeSats in-orbit electromagnetic transfer system, aimed at minimizing disturbances to the platform’s attitude caused by CubeSat transfers while also reducing the number of steps required for CubeSats to reach their designated positions.

The enhancement of the A* algorithm involves four key improvements: developing an attitude disturbance model, crafting a refined cost function, implementing a path coordination strategy, and optimizing the management of the open list. The first step involves creating a model to quantify the level of attitude disturbance on the electromagnetic conveying platform during CubeSat transfers and integrating this model into the cost function to better reflect the trade-offs between transfer efficiency and disturbance. In response to potential blockages caused by the high number of CubeSats on the platform, a path coordi-

nation strategy is introduced to effectively manage and plan the transfer route, ensuring smooth delivery of CubeSats to their target locations. To improve the efficiency of the algorithm, this study also refines how the elements in the open list are managed, enhancing the overall execution speed of the algorithm. Ultimately, the comparative analysis of the optimal transport paths demonstrates the crucial role of movable CubeSats in maintaining the stability of the platform's attitude. The improved A* algorithm plays a key role in optimizing these paths, significantly mitigating disturbances.

On the 8×8 electromagnetic conveying platform, Case 1 only involves the transfer of target CubeSats, whereas Case 2 includes both target and movable CubeSats, moving four and nine CubeSats, respectively, to the launch window. In Case 2, the platform's final angular acceleration is $0.0009 \text{ rad}\cdot\text{s}^{-2}$, its final angular velocity is $-0.0026 \text{ rad}\cdot\text{s}^{-1}$, and its maximum angular velocity reaches $-0.029 \text{ rad}\cdot\text{s}^{-1}$. In contrast, Case 1's final angular acceleration is approximately 80 times, the final angular velocity is about 77 times, and the maximum angular velocity is about 7 times that of those observed in Case 2. This stark contrast underscores the indispensable role of movable CubeSats in reducing disturbances to the platform's attitude. The improved A* algorithm specifically tailors transport path planning for the joint movement of target and movable CubeSats, ensuring a stable platform attitude and balanced transport efficiency, thereby enabling effective large-scale CubeSat in-orbit transfer path planning.

Author Contributions: Conceptualization, H.Y. and D.X.; methodology, Y.Z. (Yong Zhao); software, F.Y.; validation, J.W., X.P. and T.T.; formal analysis, Y.Z. (Yuhao Zhang); investigation, D.X.; resources, H.Y.; data curation, F.Y.; writing—original draft preparation, D.X.; writing—review and editing, Y.Z. (Yong Zhao); visualization, J.W.; supervision, X.P.; project administration, T.T.; funding acquisition, Y.Z. (Yuhao Zhang). All authors have read and agreed to the published version of the manuscript.

Funding: This research was funded by the National Natural Science Foundation of China (52075118).

Data Availability Statement: No new data were created or analyzed in this study. Data sharing is not applicable to this article.

Acknowledgments: The author would like to thank the editors, the academic editor, and the reviewers for their valuable comments and constructive suggestions that helped to improve the paper significantly.

Conflicts of Interest: The authors declare no conflicts of interest.

References

1. Liu, S.; Theoharis, P.I.; Raad, R.; Tubbal, F.; Theoharis, A.; Iranmanesh, S.; Abulgasem, S.; Khan, M.U.A.; Matekovits, L. A Survey on CubeSat Missions and Their Antenna Designs. *Electronics* **2022**, *11*, 2021. [[CrossRef](#)]
2. Fernandez, L.; Sobrino, M.; Ruiz-de-Azua, J.A.; Calveras, A.; Camps, A. Design of a Deployable Helix Antenna at L-Band for a 1-Unit CubeSat: From Theoretical Analysis to Flight Model Results. *Sensors* **2022**, *22*, 3633. [[CrossRef](#)] [[PubMed](#)]
3. Azami, M.H.b.; Orger, N.C.; Schulz, V.H.; Oshiro, T.; Cho, M. Earth Observation Mission of a 6U CubeSat with a 5-Meter Resolution for Wildfire Image Classification Using Convolution Neural Network Approach. *Remote Sens.* **2022**, *14*, 1874. [[CrossRef](#)]
4. Nason, I.; Puig-Suari, J.; Twiggs, R. Development of a Family of Picosatellite Deployers Based on the CubeSat Standard. In Proceedings of the IEEE Aerospace Conference, Big Sky, MT, USA, 9–16 March 2002; IEEE: Big Sky, MT, USA, 2002; p. 1.
5. Bernal, C.A.; van Bolhuis, M. Releasing the Cloud: A Deployment System Design for the QB50 CubeSat Mission. In Proceedings of the Small Satellite Conference, Logan, UT, USA, 14 August 2012; p. 1.
6. Puig-Suari, J.; Turner, C.; Twiggs, R.J. CubeSat: The Development and Launch Support Infrastructure for Eighteen Different Satellite Customers on One Launch. In Proceedings of the 15th Annual AIAA/USU Conference on Small Satellites, Logan, UT, USA, 13–16 August 2001.
7. Heidt, M.; Puig-Suari, J.; Moore, A.S.; Nakasuka, S.; Twiggs, R.J. CubeSat: A New Generation of Picosatellite for Education and Industry Low-Cost Space Experimentation. In Proceedings of the Thirteenth Annual AIAA/USU Small Satellite Conference, Logan, UT, USA, 23–26 August 1999.
8. Lee, S.; Toorian, A.; Clemens, N.; Puig-Suari, J.; Twiggs, B. Cal Poly Coordination of Multiple CubeSats on the DNEPR Launch Vehicle. In Proceedings of the 18th Annual AIAA/USU Conference on Small Satellites, Carefree, AZ, USA, 9–11 August 2004.
9. Mohamed, R. Design and Implementation of Ground Support Equipment for Characterizing Performance of XPOD and CNAPS & Thermal Analysis of CNAPS Pressure Regulator Valve. Master's Thesis, University of Toronto, Toronto, ON, Canada, 2009.

10. Pranajaya, F.M.; Zee, R.E. The Generic Nanosatellite Bus: From Space Astronomy to Formation Flying Demo to Responsive Space. In Proceedings of the International Conference on Advances in Satellite and Space Communications, Colmar, France, 20–25 July 2009; pp. 134–140.
11. Dobrowolski, M.; Grygorczuk, J.; Kedziora, B.; Tokarz, M.; Borys, M. Dragon-8U Nanosatellite Orbital Deployer. In Proceedings of the 42nd Aerospace Mechanisms Symposium, Baltimore, MD, USA, 14–16 May 2014; pp. 1–10.
12. Thompson, L.D. Development of a NASA 6-U Satellite. In Proceedings of the Small Satellite Conference, Logan, UT, USA, 8–11 August 2011; p. 1.
13. Akagi, H.; Takata, M.; Watanabe, H.; Sano, T.; Oikawa, K. Kibo's Contribution to Broadening the Possibilities for Micro/Nano-Satellite. In Proceedings of the SpaceOps Conferences, Daejeon, Korea, 16–20 May 2016; pp. 1–10.
14. Zhao, Y.; Yue, H.; Mu, X.; Yang, X.; Yang, F. Design and Analysis of a New Deployer for the in Orbit Release of Multiple Stacked CubeSats. *Remote Sens.* **2022**, *14*, 4205. [[CrossRef](#)]
15. Zhao, Y.; Yue, H.; Zhu, J.; Yang, X. A Planar Electromagnetic Actuator With Passive Adsorption for CubeSats Transport in a Weightless Environment. *IEEE Trans. Ind. Electron.* **2023**, *70*, 10396–10408. [[CrossRef](#)]
16. Zhao, Y.; Yue, H.; Zhu, J.; Yang, F. Armature Reaction Analysis and Suppression of Voice Coil Actuator Based on an Improved Magnetic Equivalent Circuit Model. *IEEE Trans. Ind. Electron.* **2023**, *71*, 7599–7609. [[CrossRef](#)]
17. Zhao, Y.; Yue, H.; Yang, F.; Zhu, J. A High Thrust Density Voice Coil Actuator With a New Structure of Double Magnetic Circuits for CubeSat Deployers. *IEEE Trans. Ind. Electron.* **2022**, *69*, 13305–13315. [[CrossRef](#)]
18. Tang, G.; Tang, C.; Claramunt, C.; Hu, X.; Zhou, P. Geometric A-Star Algorithm: An Improved A-Star Algorithm for AGV Path Planning in a Port Environment. *IEEE Access* **2021**, *9*, 59196–59210. [[CrossRef](#)]
19. Han, C.; Li, B. Mobile Robot Path Planning Based on Improved A* Algorithm. In Proceedings of the 2023 IEEE 11th Joint International Information Technology and Artificial Intelligence Conference (ITAIC), Chongqing, China, 8–10 December 2023; pp. 672–676.
20. Wang, H.; Lou, S.; Jing, J.; Wang, Y.; Liu, W.; Liu, T. The EBS-A* Algorithm: An Improved A* Algorithm for Path Planning. *PLoS ONE* **2022**, *17*, e0263841. [[CrossRef](#)] [[PubMed](#)]
21. Liu, C.; Mao, Q.; Chu, X.; Xie, S. An Improved A-Star Algorithm Considering Water Current, Traffic Separation and Berthing for Vessel Path Planning. *Appl. Sci.* **2019**, *9*, 1057. [[CrossRef](#)]
22. Fan, G.; Xing, X.; Han, Y.; Chen, M.; Gui, H. Path Planning for Ground Target Reconnaissance Based on Improved Astar Algorithm. In Proceedings of the 2021 China Automation Congress (CAC), Beijing, China, 22–24 October 2021; pp. 2092–2097.
23. Fan, Y.; Deng, F.; Shi, X. Multi-Robot Task Allocation and Path Planning System Design. In Proceedings of the 2020 39th Chinese Control Conference (CCC), Shenyang, China, 27–29 July 2020; pp. 4759–4764.
24. Li, M.; Qiao, L.; Jiang, J. A Multigoal Path-Planning Approach for Explosive Ordnance Disposal Robots Based on Bidirectional Dynamic Weighted-A* and Learn Memory-Swap Sequence PSO Algorithm. *Symmetry* **2023**, *15*, 1052. [[CrossRef](#)]
25. Ou, Y.; Fan, Y.; Zhang, X.; Lin, Y.; Yang, W. Improved A* Path Planning Method Based on the Grid Map. *Sensors* **2022**, *22*, 6198. [[CrossRef](#)] [[PubMed](#)]
26. Kılıç, Ç.; Scholz, T.; Asma, C. Deployment Strategy Study of QB50 Network of CubeSats. In Proceedings of the 6th International Conference on Recent Advances in Space Technologies (RAST), Istanbul, Turkey, 12–14 June 2013; pp. 935–939.
27. Jeyakumar, D.; Rao, B.N. Dynamics of Satellite Separation System. *J. Sound Vib.* **2006**, *297*, 444–455. [[CrossRef](#)]
28. Handschuh, D.D.A.; Bourgeois, E. Optimization of Constellation Jettisoning Regards to Short Term Collision Risks. *Acta Astronaut.* **2018**, *145*, 284–292. [[CrossRef](#)]

Disclaimer/Publisher's Note: The statements, opinions and data contained in all publications are solely those of the individual author(s) and contributor(s) and not of MDPI and/or the editor(s). MDPI and/or the editor(s) disclaim responsibility for any injury to people or property resulting from any ideas, methods, instructions or products referred to in the content.